# A cooperative insertion mechanism for efficient $CO_2$ capture in diamine-appended metal-organic frameworks

Thomas M. McDonald[1], Jarad A. Mason[1], Xueqian Kong[2,3,4], Eric D. Bloch[1], David Gygi[1], Alessandro Dani[5], Valentina Crocellà[5], Filippo Giordanino[5], Samuel Odoh[6], Walter Drisdell[7], Bess Vlaisavljevich[2], Allison L. Dzubak[6], Roberta Poloni[8], Sondre K. Schnell[2,9], Nora Planas[6], Lee Kyuho[7], Tod Pascal[7], Liwen F. Wan[7], David Prendergast[7], Jeffrey B. Neaton[7], Berend Smit[2,7], Jeffrey B. Kortright[7], Laura Gagliardi[6], Silvia Bordiga[5], Jeffrey A. Reimer[2,3] & Jeffrey R. Long[1,10]

**Advanced solid adsorbents have the potential to decrease significantly the cost of $CO_2$ removal from the effluent streams of fossil fuel-burning power plants. Here, we demonstrate that the diamine-appended metal-organic frameworks mmen-$M_2$(dobpdc) (mmen = *N*,*N*′-dimethylethylenediamine; M = Mg, Mn, Fe, Co, Zn; dobpdc$^{4-}$ = 4,4′-dioxidobiphenyl-3,3′-dicarboxylate) behave as "phase-change" adsorbents, exhibiting unusual step-shaped $CO_2$ adsorption isotherms that shift dramatically with temperature. Based upon spectroscopic, diffraction, and computational studies, the origin of the sharp adsorption step is attributed to an unprecedented cooperative process in which, above a metal-dependent threshold pressure, $CO_2$ molecules insert into metal-amine bonds, inducing a reorganization of the amines into well-ordered chains of ammonium carbamate. As a result, separation capacities in excess of 10 wt % can be achieved using temperature swings of as little as 50 °C. Adsorbent regeneration energies 20-40% lower than those achievable employing state-of-the-art aqueous amine solutions are shown to be feasible, with additional savings in the cost of carbon capture attainable if $CO_2$ removal from the flue gas can be effected at temperatures near 100 °C. These results provide a mechanistic framework for designing new, highly-efficient adsorbents for removing $CO_2$ from various gas mixtures, while further exposing important structural insights into the conservation of $Mg^{2+}$ within the RuBisCO family of enzymes.**

[1]Department of Chemistry, University of California, Berkeley CA 94720, USA. [2]Department of Chemical and Biological Engineering, University of California, Berkeley CA 94720, USA. [3]Environmental Energy Technologies Division, Lawrence Berkeley National Laboratory, Berkeley, CA 94720, USA. [4]Department of Chemistry, Zhejiang University, Hangzhou 310027, China. [5]Chemistry Department, NIS and INSTM Centre of Reference, University of Turin, Via Quarello 15, I-10135 Torino, Italy. [6] Department of Chemistry, Chemical Theory Center, and Supercomputing Institute, University of Minnesota, Minneapolis, MN 55455, USA. [7]Molecular Foundry, Lawrence Berkeley National Laboratory, One Cyclotron Road, Berkeley, California, 94720, USA. [8]Laboratoire de Science et Ingeniente des Materiaux et Procedes (SIMaP), UMR CNRS 5266. Grenoble-INP, BP 75, 38402 Saint Martin d'Heres Cedex, France. [9]Department of Chemistry, Norwegian University of Science and Technology, Høgskoleringen 5, 7149 Trondheim, Norway. [10]Materials Sciences Division, Lawrence Berkeley National Laboratory, Berkeley, CA 94720, USA.

Exceeding 13 gigatons annually[1], carbon dioxide generated from the combustion of fossil fuels for heat and electricity production is a major contributor to climate change and ocean acidification[2,3]. Implementation of carbon capture and sequestration technologies has been proposed as a means of enabling the continued use of fossil fuels in the near term, while renewable energy sources gradually replace our existing infrastructure[4]. The removal of $CO_2$ from low-pressure flue gas mixtures is presently effected by aqueous amine solutions that are highly selective for acid gases[5]. As a result of the large energy penalty for desorbing $CO_2$ from such liquids, solid adsorbents with significantly lower heat capacities are frequently proposed as promising alternatives[6,7]. In particular, owing to their high surface areas and tunable pore chemistry, the separation capabilities of certain metal-organic frameworks have been shown to meet or exceed those achievable by zeolite or carbon adsorbents[8-10].

Recently, the attachment of alkyldiamines to coordinatively-unsaturated metal sites lining the pores of selected metal-organic frameworks has been demonstrated as a facile methodology for increasing low pressure $CO_2$ adsorption selectivity and capacity[11-14]. Most notably, functionalization of $Mg_2$(dobpdc) (dobpdc$^{4-}$ = 4,4′-dioxidobiphenyl-3,3′-dicarboxylate), an expanded variant of the well-studied metal-organic framework $Mg_2$(dobdc) (dobdc$^{4-}$ = 2,5-dioxidobenzene-1,4-dicarboxylate)[15-18], with *N*,*N*′-dimethylethylenediamine (mmen) generated an adsorbent with exceptional $CO_2$ capacity under flue gas conditions and unusual, unexplained step-shaped adsorption isotherms[13]. Here, we elucidate the unprecedented mechanism giving rise to these step-shaped isotherms and demonstrate that replacing $Mg^{2+}$ with other divalent metal ions enables the position of the $CO_2$ adsorption step to be manipulated in accord with the metal-amine bond strength. As we will show, the resulting mmen-$M_2$(dobpdc) (M = Mg, Mn, Fe, Co, Zn) compounds, hereby denominated "phase-change" adsorbents, can exhibit highly desirable

characteristics that make them superior to other solid or liquid sorbents for the efficient capture of $CO_2$.

Fig. 1 illustrates the extraordinary advantages associated with utilizing an adsorbent exhibiting step-shaped isotherms in a temperature swing adsorption process versus the Langmuir-type isotherms observed for most microporous adsorbents. To our knowledge, these advantages have not previously been recognized. For carbon capture applications, a gas mixture containing $CO_2$ at low pressure ($P_{ads}$) and low temperature ($T_{low}$) is contacted with the adsorbent, which selectively adsorbs a large amount of $CO_2$. The adsorbent is heated to liberate pure $CO_2$ with a partial pressure of $P_{des}$, and then reused for subsequent adsorption/desorption cycles. For a classical adsorbent (Fig. 1a), including all previous amine-based sorbents, the steepness of the isotherm gradually diminishes as the temperature increases, necessitating a high desorption temperature to achieve a significant working capacity for a separation. In contrast, for a phase-change adsorbent of the type investigated here (Fig. 1b), the position of the isotherm step shifts dramatically to higher pressures as the temperature increases, such that a large working capacity can be achieved with only a small increase in temperature. For an efficient carbon capture process, one would ideally create a phase-change adsorbent with a large vertical step positioned just below the partial pressure of $CO_2$ in the flue gas.

## Cooperative insertion of $CO_2$ into metal-amine bonds

Spectroscopic and diffraction measurements were undertaken to determine the mechanism of $CO_2$ uptake leading to a steep adsorption step for adsorbents such as mmen-$Mg_2$(dobpdc). In particular, powder x-ray diffraction studies, which were performed on the isostructural compound mmen-$Mn_2$(dobpdc) owing to the greater crystallinity of its base framework, provided detailed structural information on how $CO_2$ binds within the channels of the material. Diffraction data collected at 100 K before and after exposure of a sample to 5 mbar of $CO_2$ show the unit cell volume to contract by just 1.112(8)%, but revealed significant changes in the relative intensity of selected diffraction peaks (Fig. 4a). Complete structural models were developed for both data sets using the simulated annealing method, as implemented in TOPAS-Academic[19], followed by Rietveld refinement against the data (Figs. 2a-b). Before $CO_2$ exposure, the mmen molecules are bound via one amine group to the $Mn^{2+}$ sites with a Mn−N distance of 2.29(6) Å, while the other amine lies exposed on the surface of the framework (Fig. 2c). Counter to our initial assumption that the uncoordinated amine groups would serve to bind $CO_2$[13,20], $CO_2$ adsorption instead occurs

via full insertion into the Mn−N bond, resulting in a carbamate with one O atom bound to Mn at a distance of 2.10(2) Å (Fig. 2d). Notably, the second O atom of the carbamate has a close interaction of 2.61(9) Å with the N atom of a neighboring mmen, resulting in chains of ammonium carbamate running along the *c* axis of the structure (Fig 2e). The observed ammonium carbamate N···O distance is similar to the distance of 2.66-2.72 Å in a single crystal of pure mmen-$CO_2$ (methyl(2-(methylammonio)ethyl)carbamate)[21]. Importantly, this well-ordered chain structure is maintained at 295 K, as determined from a full Rietveld refinement against data collected at this temperature (Fig. X). Thus, the adsorption of $CO_2$ at ambient temperatures is associated with a structural transition to form an extended chain structure held together by ion-pairing between the metal-bound carbamate units and the outstretched ammonium group of a neighboring mmen molecule.

The foregoing structural information enables formulation of a detailed mechanism for the adsorption of $CO_2$ in phase change adsorbents of the type mmen-$M_2$(dobpdc). As shown in Fig. 3, the uncoordinated amine of a mmen molecule acts as a strong base to remove the acidic proton from the metal-bound amine of a neighboring mmen molecule. Deprotonation occurs only in the presence of $CO_2$, such that simultaneous nucleophilic addition of $CO_2$ results in the formation of a carbamate with an associated ammonium countercation. At suitable temperatures and pressures, rearrangement of the carbamate is possible such that the M–N bond is broken and a M–O bond is formed. Critically, the ion-pairing interaction causes the mmen molecule to stretch, destabilizing the M–N bond and facilitating insertion at the next metal site. This cooperative effect will propagate until a complete one-dimensional ammonium carbamate chain has formed. Indeed, it is this cooperativity that leads to the sudden uptake of a large amount of $CO_2$ and a steep vertical step in the adsorption isotherm.

Infrared spectroscopy measurements performed on mmen-$Mg_2$(dobpdc) fully support the proposed mechanism. As shown in Fig. 4b, significant changes to the infrared spectrum are apparent upon isobarically cooling a sample of the compound from 150 to 30 °C at 1 °C/min under a flowing 5% $CO_2$ in $N_2$ atmosphere. At high temperatures, two distinct N–H vibrations arise at 3258 and 3334 $cm^{-1}$, which are also present in the spectrum of mmen-$Mg_2$(dobpdc) in the absence of $CO_2$ and can be attributed to the coordinated and uncoordinated ends of mmen, respectively. Upon cooling, both of these N–H resonances disappear, indicating significant changes to both amines of mmen, while a new, extremely broad N-H band characteristic of ammonium formation appears (Fig. X). From the weak, but clearly discernable C=O vibration at

1690 $cm^{-1}$, carbamate formation between mmen and $CO_2$ occurs under all conditions, even at high temperatures. However, an additional sharp band at 1334 $cm^{-1}$, corresponding to the C–N vibrational mode of a carbamate, is only observed upon cooling below 110 °C. The delayed onset of this easily recognizable band, which is diagnostic of a phase-change adsorbent of the type investigated here, is attributable to changes in the resonance configuration of carbamate that occur upon coordination of one of its O atoms. The normalized intensities of the C–N band and a second band at 658 $cm^{-1}$ versus temperature demonstrate that their formation are directly related to the sharp step in the gravimetric adsorption isobar measured under identical experimental conditions. From the infrared spectra, it is clear that, while a small amount of $CO_2$ can adsorb via ammonium carbamate formation between pairs of adjacent amines, it is specifically the adsorption of $CO_2$ to form ammonium carbamate chains that endows these materials with their step-change adsorption properties.

To better understand the step-wise pathway by which the amines initially adsorb $CO_2$, DFT calculations were paired with *in situ* Near Edge X-ray Absorption Fine Structure (NEXAFS) measurements of the nitrogen K-edge of mmen-$Mg_2$(dobpdc) collected under increasing $CO_2$ pressure (Fig. 4c)[22], and all observed spectral changes were accurately reproduced by computed spectra. From the NEXAFS spectra, the new pre-edge peak at 402.3 eV arises solely from the carbamate nitrogen and is a clear signature of carbamate insertion into the metal-nitrogen bond. As in infrared spectroscopy, this feature is attributable to resonance of the nitrogen lone pair into the π system of the carbamate after the coordinate bond utilizing the same electron pair with the Mg metal centre has been broken. A second new, broad feature between 411 and 419 eV also arises solely from the carbamate nitrogen and is a signature of the new N-C bond formed upon $CO_2$ adsorption. This feature appears prior to insertion and is general to both terminal-bound and inserted carbamate moieties. Finally, the ~1 eV blueshift of the main edge peak at 405.4 eV is characteristic of ammonium formation.

Solid-state NMR spectra indicate that $CO_2$ adsorption significantly affects the manner in which diamines coordinate to the metal sites of the framework (Fig. 4d). Upon exposure of mmen-$Mg_2$(dobpdc) to $CO_2$, $^{15}N$ chemical shifts consistent with ammonium and carbamate are observed at 31 and 72 ppm, respectively. Yet, surprisingly, only a single $^{15}N$ resonance is apparent for mmen-$Mg_2$(dobpdc) in the absence of $CO_2$. This indicates that the coordinated and uncoordinated ends of the mmen molecules are capable of interconverting on the timescale of the NMR experiment, although, as discussed above, they are distinguishable on the much faster

timescale of infrared spectroscopy. Despite being labile, the amines are stable to evacuation under vacuum at high temperatures. This unexpected lability appears to allow substitution, but not elimination, reactions to occur rapidly under conditions relevant to carbon capture. Furthermore, the sudden adsorption of $CO_2$ in this compound is thus associated with a transition from a dynamic surface state to a well-ordered extended surface structure. Accordingly, the reaction with $CO_2$ can be considered to be thermodynamically nonspontaneous at low pressures because of the large positive entropy associated with this transition. Indeed, the molar entropy of gas phase $CO_2$ was found to be the primary determinant of the step pressure for phase-change adsorbents. As shown in Fig. S, step pressures for all five phase-change metal organic frameworks are linearly correlated with the gas phase entropy of $CO_2$ as a function of temperature.

## Understanding and manipulating the isotherm steps

The mechanism of $CO_2$ adsorption suggests that variation of the metal-amine bond strength should provide a means of manipulating the isotherm step position. The series of isostructural compounds mmen-$M_2$(dobpdc) (M = Mg, Mn, Fe, Co, Ni, Zn) were therefore synthesized, and the $CO_2$ adsorption isotherms for each were measured at 25, 40, 50, and 75 °C (Fig. 5). With the exception of the Ni compound, which exhibits normal Langmuir-type adsorption behavior (Fig. 5e), all of the materials display sharp isotherm steps that shift to higher pressure with increasing temperature. Analysis of the isotherm steps at 25 °C affords Hill coefficients[23] of 10.6, 5.6, 7.5, 11.5, and 6.0 for M = Mg, Mn, Fe, Co, and Zn, respectively, clearly reflecting the cooperative nature of the $CO_2$ adsorption mechanism. Simulated isotherms generated from Grand Canonical Monte Carlo (GCMC) simulations using a simple lattice model capture the experimentally observed isotherm step only when all mmen groups react with $CO_2$ and align down the crystallographic *c*-axis (Fig. SX).

For a given temperature, the step position varies in the order Mg < Mn < Fe < Zn < Co, in good agreement with the series of Irving and Williams for octahedral metal complex stabilities[24]. The lack of a step for the Ni compound, even at very high pressures (Fig. X), is attributable to the exceptional stability of the Ni–mmen bond, which prevents carbamate insertion from taking place under the conditions surveyed. Geometry optimizations performed at the DFT/PBE[25] level confirm that calculated adsorption energies, which are in good agreement with experimentally calculated values, are directly correlated with the calculated metal–amine bond length (Fig. X).

Thus, we anticipate that similar variations in tuning step position will be possible by altering the sterics of the amine bound to the metal, as well as the spacer between the two amine groups. Hence, depending on the concentration of $CO_2$ present in a gas mixture, an adsorbent can be rationally designed to match the optimum process conditions depicted in Fig. 1.

While stepped adsorption isotherms[26] have been observed previously in solid adsorbents, the origin of the step reported here is distinctly unique from all previously reported mechanisms. First, in contrast to most metal-organic frameworks exhibiting such behaviour, the isotherm steps reported here are not attributable to pore opening, gate opening, or pore closing processes[27-29]. For mmen-$Mn_2$(dobpdc), only a ~1% decrease in the unit cell volume was observed upon $CO_2$ adsorption, and from Figs. 2a-b, it is apparent that the entire pore surface is accessible to $CO_2$ throughout the adsorption isotherm. A gate opening mechanism attributable to the rearrangement of flexible hydrogen-bonding functional groups, which function by preventing $CO_2$ diffusion into the pores at low partial pressures[30], cannot explain the presence of distinct adsorption steps when the material is slowly cooled from high to low temperatures under isobaric adsorption conditions (*vide infra*). Second, in contrast to adsorbed-layer phase transitions on highly homogenous surfaces, the adsorbed phase reported here is stable at temperatures well above the critical temperature of $CO_2$[31]. Third, the phase transition is a metal cation-dependent, solid-to-solid transformation, in contrast to liquid-to-liquid or liquid-to-solid phase change reactions typically reported for amine–$CO_2$ systems[32-34]. Lastly, under conditions relevant to $CO_2$ capture, desorption hysteresis is minimal, because the sharp steps occur over a narrow pressure regime and the adsorption and desorption onset points are at approximately the same temperature and pressure (Fig. X).

A number of features unique to the mmen-$M_2$(dobpdc) series allow for phase transitions of this type to be observed for the first time. First, for solid ammonium carbamate chains to form, the metal–amine coordinate bond must be capable of rearrangement. Thus, only adsorbents tethered to the solid surface through coordinate bonds rather than covalent bonds can undergo the mechanism reported here. Second, a homogenous surface with appropriately positioned adsorption sites, which is dictated by the location of open metal sites within the pores of the metal-organic framework, is necessary. Thus, a very limited number of metal-organic framework materials will be able to mimic the adsorption behaviour reported here, and it is likely that no amine-functionalized mesoporous silica sorbent can be engineered precisely enough to meet these requirements. Remarkably, while the pore expanded derivatives of $M_2$(dobdc) reported

here exhibit these properties, amine functionalization of the original $Mg_2$(dobdc) compound was not reported to result in stepped adsorption isotherms[35].

## Low-energy carbon capture applications

Effective adsorbents for carbon capture must possess large working capacities for processes occurring at temperatures above 40 °C and at $CO_2$ partial pressures near 0.15 bar for coal flue gas or near 0.05 bar for a natural gas flue stream. On this basis, the location of the isotherm steps for the Mg and Mn compounds makes them better suited for this application than the Fe, Co, and Zn compounds, which are better suited for separations from gas mixtures with higher $CO_2$ concentrations. To assess the utility of these phase-change adsorbents for capturing $CO_2$ in a pure temperature swing adsorption process, adsorption isobars were collected under dynamic gas flow. Samples of mmen-$Mg_2$(dobpdc) and mmen-$Mn_2$(dobpdc) were activated, saturated with 100% $CO_2$, and then isobarically cooled to room temperature under three different $CO_2$ containing gas mixtures: 100%, 15%, and 5%. The resulting isobars, shown in Figs. 6a-b, reveal how small changes in temperature induce large changes in the quantity of $CO_2$ adsorbed. As shown in Figs. 6c-d, phase-change adsorbents exhibit very large working capacities when utilized in temperature swing adsorption (TSA) processes. For mmen-$Mg_2$(dobpdc) to exhibit a working capacity in excess of 13 wt %, the material must simply swing between 100 and 150 °C. Similarly, the working capacity of mmen-$Mn_2$(dobpdc) is in excess of 10 wt.% when cycled between 70 and 120 °C. Of particular note, to accurately simulate a pure TSA process, 15% $CO_2$ in $N_2$ was flowed over the samples during the cooling phase, while 100% $CO_2$ was used during heating phases. In contrast to experiments that utilize a purge gas to assist $CO_2$ desorption, no inert gases were used to regenerate the samples.

Estimations based upon differential scanning calorimetry, thermogravimetric analysis, and isosteric heat determinations indicate that mmen-$Mg_2$(dobpdc) and mmen-$Mn_2$(dobpdc) can achieve regeneration energies of approximately 2.2 MJ per kg of $CO_2$ captured. This value is significantly lower than the regeneration energies attainable utilizing monoethanolamine (3.5 MJ/kg) or even state-of-the-art amines, such as piperazine and KS-1 (2.6 MJ/kg)[5,36]. In contrast to aqueous amine absorbents that utilize heat exchangers to save sensible energy costs, the significantly greater working capacities and smaller temperature swings of phase-change adsorbents allow more economical processes to be developed for a high-enthalpy adsorbent without the use of a heat exchanger. Because phase-change adsorbents saturate with $CO_2$ at their

transition point, it is not necessary for adsorption to occur at the lowest possible temperature. While we previously showed that mmen-$Mg_2$(dobpdc) can effectively operate under standard flue gas adsorption conditions (40 °C)[13], Fig. 6 demonstrates for the first time that phase-change adsorbents operate more efficiently at higher adsorption temperatures than at lower temperatures. Because classical adsorbents must operate at the lowest possible adsorption temperature to maximize working capacity, only phase-change adsorbents can enable high-temperature adsorption processes to be considered for the first time.

Adsorbing $CO_2$ at elevated temperatures affords a number of additional process benefits besides directly reducing sorbent regeneration energy. In particular, overcoming the competitive adsorption of water vapor, which is present in flue gas at high concentrations, presents a serious challenge for solid adsorbents. Amine-based solid adsorbents fare better than those utilizing a purely physical adsorption mechanism, because they are known to retain their affinity for $CO_2$ under humid conditions[37], as also demonstrated here for mmen-$Mg_2$(dobpdc) (Fig. S22). However, even for systems where the amine reactivity with $CO_2$ is unaffected by the presence of water, the physical adsorption of water onto non-amine binding sites significantly increases the overall regeneration energy of the material[38]. As shown in Fig. SX, mmen-$Mg_2$(dobpdc) adsorbs nearly 90% less water at 100 °C than at 40 °C. Thus, the energy penalty associated with desorbing co-adsorbed water can be significantly reduced by carrying out $CO_2$ adsorption at a high temperature, obviating the need for strict flue gas dehumidification. Importantly, no changes to the $CO_2$ adsorption isotherm were apparent after water exposure at 40 or 100 °C (Fig. S24), indicating the stability of the mmen-$Mg_2$(dobpdc) in the presence of water vapor even at high temperatures.

The high effective operating temperatures of mmen-$Mg_2$(dobpdc) and mmen-$Mn_2$(dobpdc) offer opportunities for cost savings beyond just reductions in the regeneration energy. Owing to the exothermic nature of all adsorption processes, the incorporation of labor and material intensive coolant pipes into an adsorbent bed (a component of the significant infrastructure cost for carbon capture) is necessary to maintain isothermal adsorption conditions. The rate of heat transfer from a sorbent bed to the coolant pipes, which contain surface temperature water at ~25 °C, is primarily dependent upon the heat transfer coefficient of the sorbent, the total contact area between the sorbent and the coolant pipes, and the temperature differential between the sorbent and the coolant[39]. The physical size of adsorption units is dictated, to a great extent, by the need to provide sufficient contact area between the coolant and sorbent for effective heat

removal. For processes that are limited by heat transfer rather than mass transfer, which is likely for many $CO_2$ capture processes utilizing solid adsorbents, the use of high temperatures will maximize the temperature differential between the coolant and the sorbent, significantly reducing the overall bed size by reducing the size of the necessary contact area. By increasing the coolant-sorbent temperature differential from approximately 15 °C to nearly 75 °C, adsorption bed size could potentially be reduced five-fold. In turn, smaller adsorbent beds would reduce the pressure drop across the adsorbent, reduce the size and cost of the required capital equipment, and allow up to five times less adsorbent to be used. By reducing these other system costs, new classes of adsorbents have the ability to reduce substantially the cost of carbon capture beyond simply reducing the sorbent regeneration energy.

## A functional model for RuBisCo

Finally and quite unexpectedly, the reactivity trends of the $M_2$(dobpdc) series may help to elucidate the evolutionary conservation of $Mg^{2+}$ within the active site of most photosynthetic enzymes. Biological fixation of atmospheric $CO_2$ is primarily effected by the ribulose-1,5-bisphosphate carboxylase/oxygenase (RuBisCO) enzyme. Striking structural similarities exist between mmen-$Mg_2$(dobpdc) and the enzymatic pocket of RuBisCO, which in its active form also contains an octahedral $Mg^{2+}$ ion ligated by five oxygen donor ligands and a reactive aliphatic amine ligand that adsorbs gas-phase $CO_2$ to form an O-bound carbamate ligand (Fig. S25)[40,41]. While other divalent metal ions can be incorporated into either structure, in each case the presence of $Mg^{2+}$ greatly enhances the reactivity for $CO_2$ fixation at very low $CO_2$ concentrations[42]. Although further study is necessary, the trends we observe suggest that the inclusion of $Mg^{2+}$ within the active site of RuBisCO is necessary to endow the lysine residue that forms the enzymatically competent carbamate-ligated metal with maximum reactivity at the very low $CO_2$ partial pressures present in air.

**Online Content** Methods, along with any additional Extended Data display items and Source Data, are available in the online version of the paper; references unique to these sections appear only in the online paper.

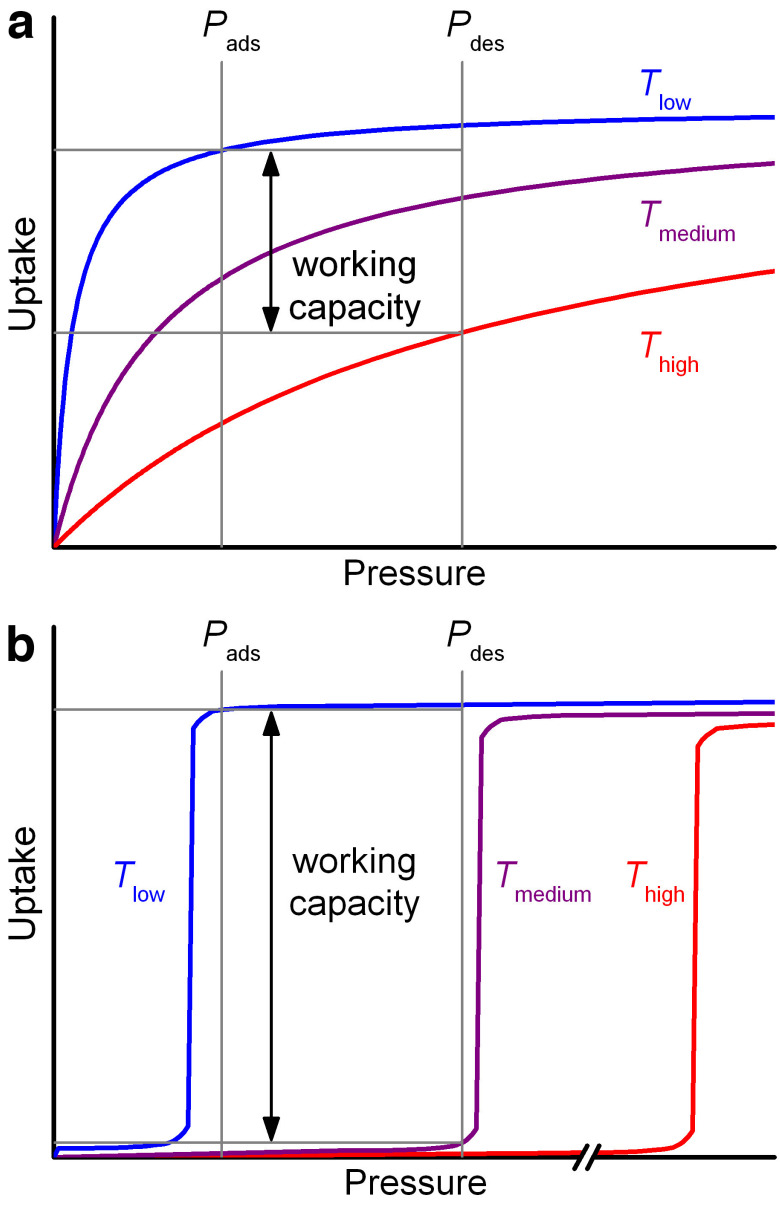


**Figure 1 | Idealized $CO_2$ adsorption isotherms.** Variation in the idealized adsorption isotherm behavior with temperature for a classical microporous adsorbent (**a**), exhibiting the usual Langmuir-type isotherm shape, versus that of a phase-change adsorbent (**b**), exhibiting step-shaped (sometimes referred to as "S-shaped") isotherms. The double-headed black arrow indicates the working capacity (i.e., the amount of gas removed) for a separation carried out using a temperature swing adsorption process in which selective adsorption occurs at $P_{ads}$ and $T_{low}$ and desorption is performed at $P_{des}$ and $T_{high}$ (**a**) or $T_{medium}$ (**b**).

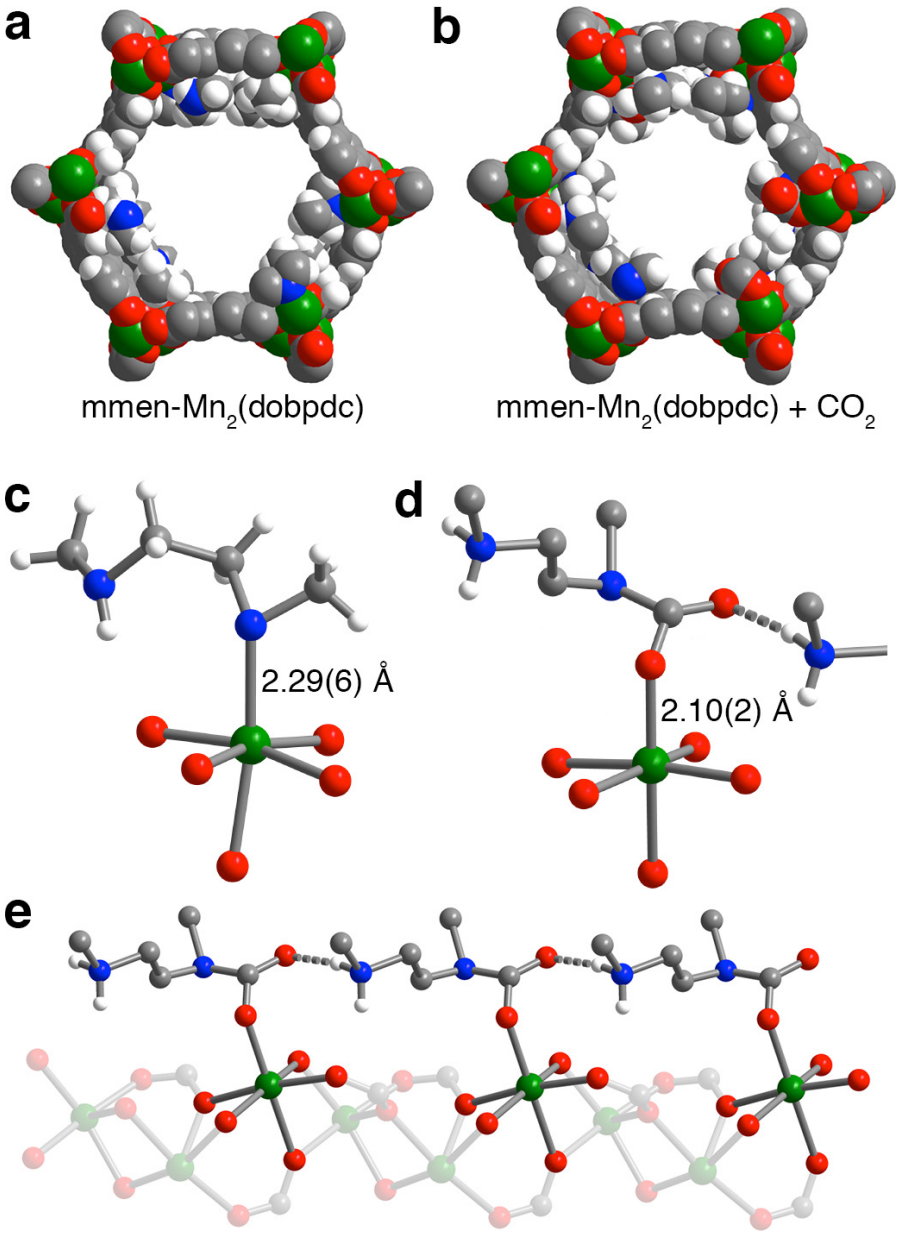


**Figure 2 | Powder x-ray diffraction structures of mmen-$Mn_2$(dobpdc).** **a**, A portion of the crystal structure for mmen-$Mn_2$(dobpdc) prior to $CO_2$ adsorption, as determined from powder x-ray diffraction data. **f**, A portion of the crystal structure for the final state of $CO_2$ adsorbed within mmen-$Mn_2$(dobpdc), as determined from powder x-ray diffraction data. Only one segment of the one-dimensional ammonium carbamate chains that form within the channels of the structure is shown. **g**, Space-filling models of the solid-state structures of mmen-$Mn_2$(dobpdc) (left) and $CO_2$-mmen-$Mn_2$(dobpdc) (right) at 100 K. Green, gray, red, blue, and white spheres represent Mn, C, O, N, and H atoms, respectively; some H atoms are omitted for clarity.

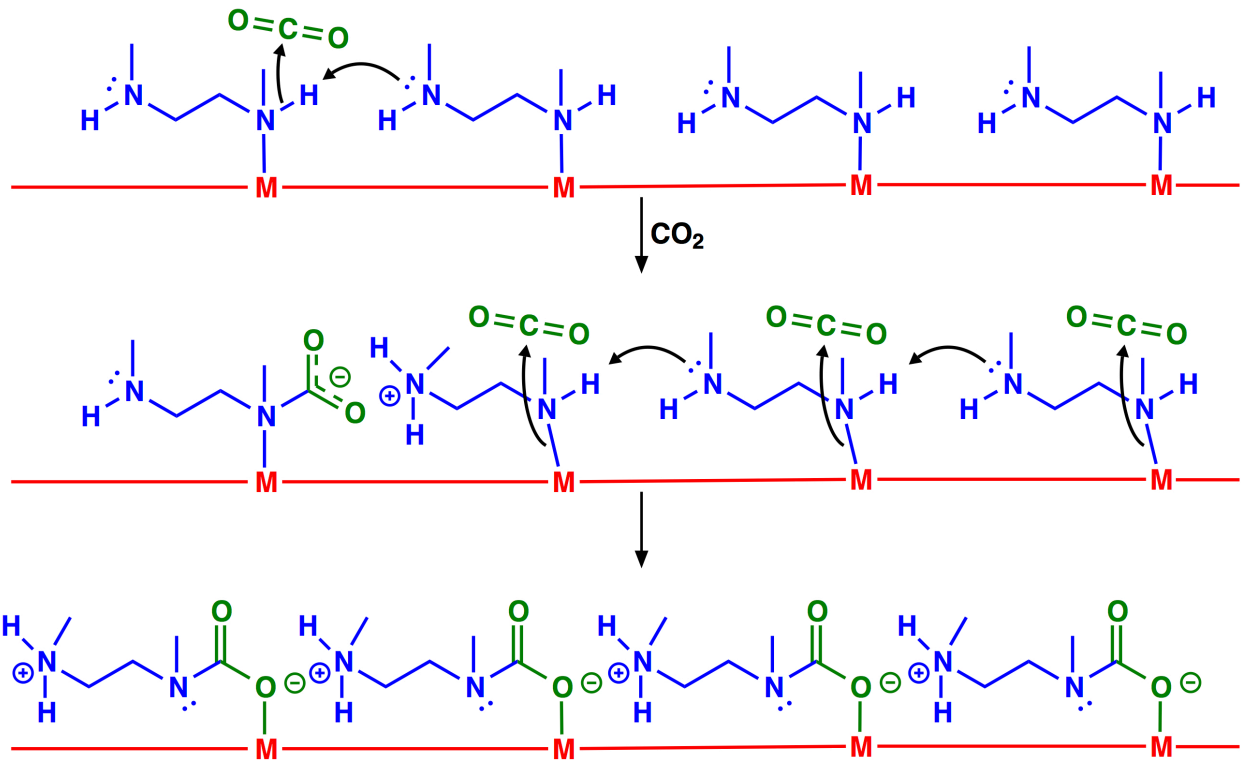


**Figure 3 | A cooperative insertion mechanism for $CO_2$ adsorption.** Depiction of the mechanism for $CO_2$ adsorption at four neighbouring M–mmen sites within an infinite one-dimensional chain of such sites running along the crystallographic *c* axis of a mmen-$M_2$(dobpdc) compound. Simultaneous proton transfer and nucleophilic attack of N on a $CO_2$ molecule forms an ammonium carbamate species that destabilizes the amine coordinated at the next metal site, initiating the cooperative adsorption of $CO_2$ via a chain reaction.

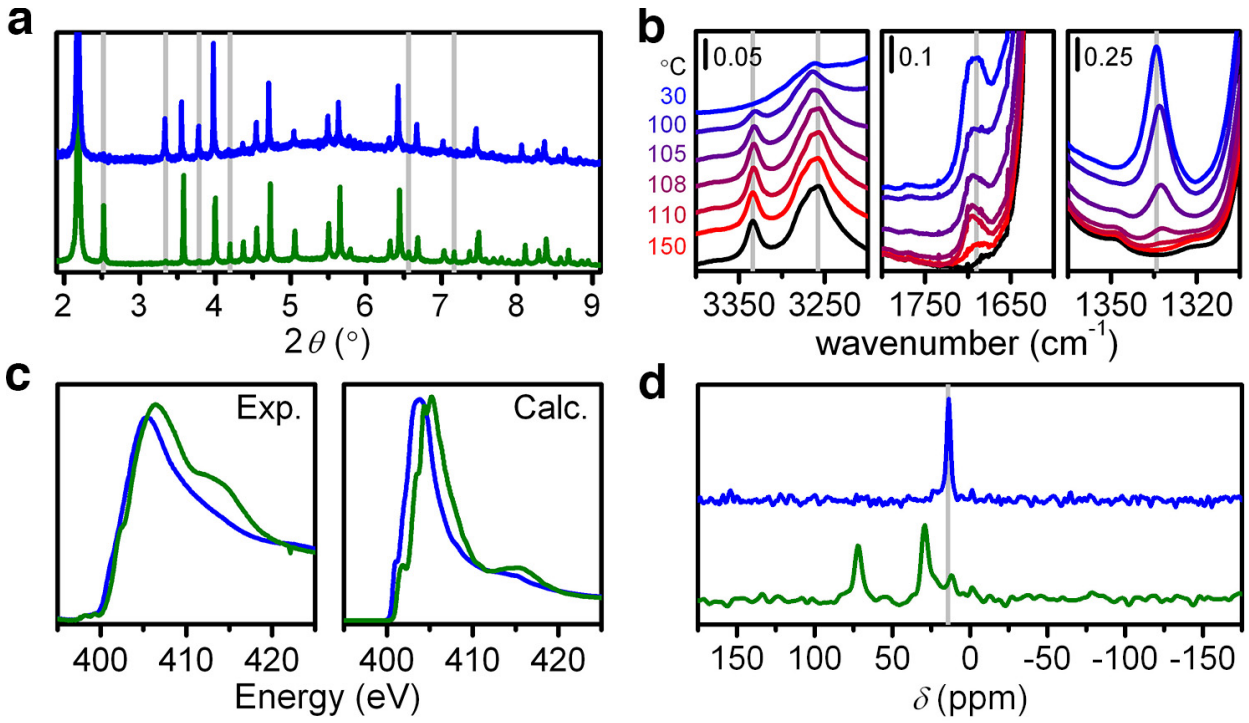


**Figure 4** | **Experimental characterization of the adsorption mechanism. a,** Large intensity differences are apparent in the powder x-ray diffraction patterns (collected at 100 K) upon exposure of mmen-$Mn_2$(dobpdc) (blue) to 5 mbar $CO_2$ (green). **b**, Infrared spectra upon dosing an activated sample of mmen-$Mg_2$(dobpdc) (black) with $CO_2$ and cooling from 150 to 30 °C (red to blue) under 5% $CO_2$ in $N_2$. The three different regions show bands corresponding to N–H, C–O, and C–N stretching vibrations, from left to right, respectively. Spectra in the left tile are artificially offset by 0.05 a.u. to aid visualization. Note that those in the other two tiles are not offset, and here $CO_2$ adsorption is responsible for the rise in the spectral baseline due to molecular charge delocalization of the ammonium carbamate chains. Complete infrared spectra can be found in Fig. S35. **c**, Experimental (left) and computational (right) NEXAFS spectra of mmen-$Mg_2$(dobpdc) at the N K-edge, before (blue) and after $CO_2$ adsorption (green); all major spectral changes are reproduced. **d**, Solid-state $^{15}N$ NMR spectra for mmen-$Mg_2$(dobpdc) before (blue) and after (green) exposure to $CO_2$ at 25 °C.

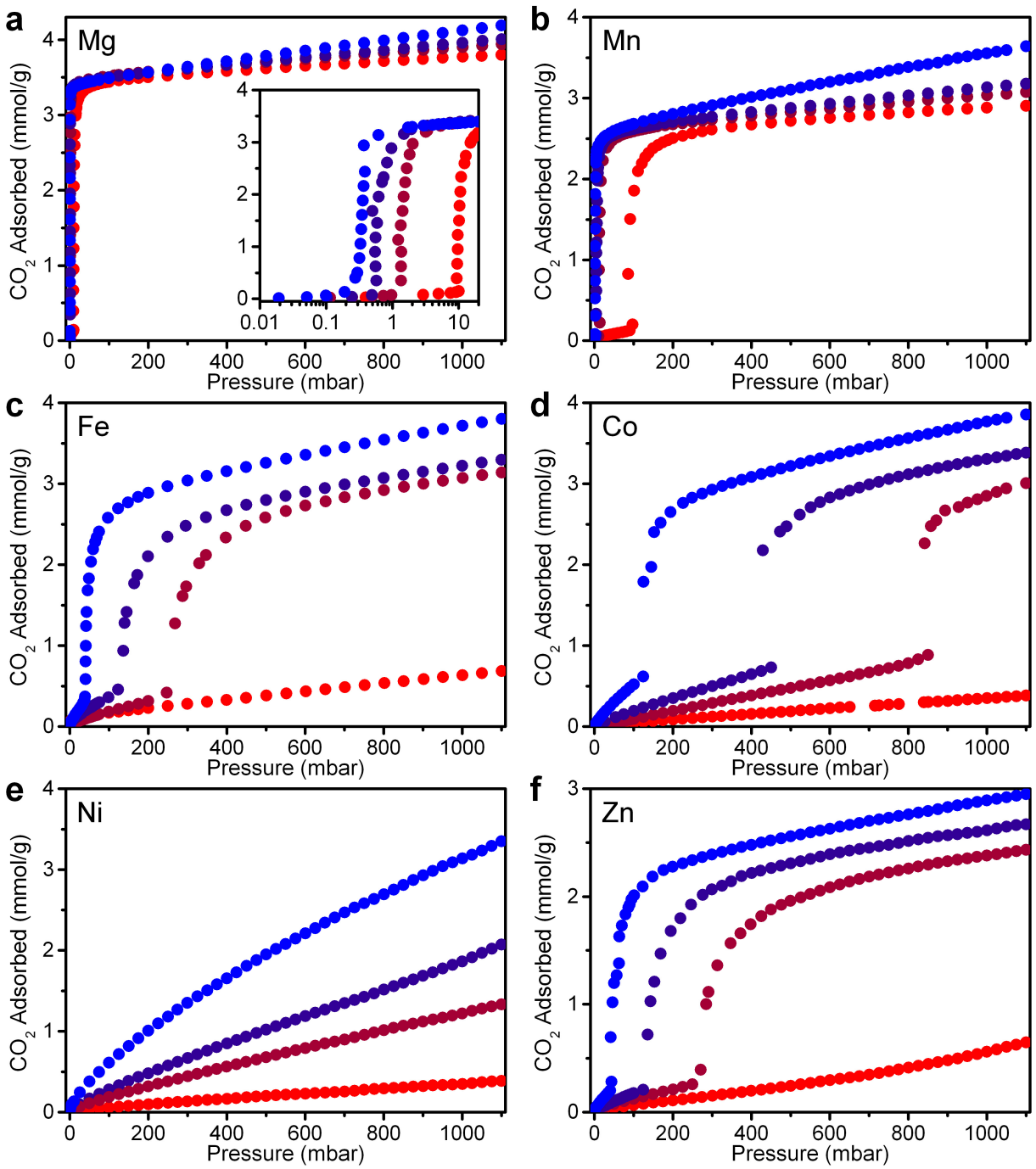


**Figure 5 | $CO_2$ adsorption isotherms.** Carbon dioxide adsorption isotherms at 25 (blue), 40 (blue-violet), 50 (red-violet), and 75 °C (red) for (**a**) mmen-$Mg_2$(dobpdc) (**b**) mmen-$Mn_2$(dobpdc) (**c**) mmen-$Fe_2$(dobpdc) (**d**) mmen-$Co_2$(dobpdc) (**e**) mmen-$Ni_2$(dobpdc) and (**f**) mmen-$Zn_2$(dobpdc). Despite the utilization of aliphatic amine groups as the $CO_2$ reactive species, the metal-organic framework plays an essential role in determining isotherm shape, owing to the importance of metal-ligand reorganization reactions in the mechanism.

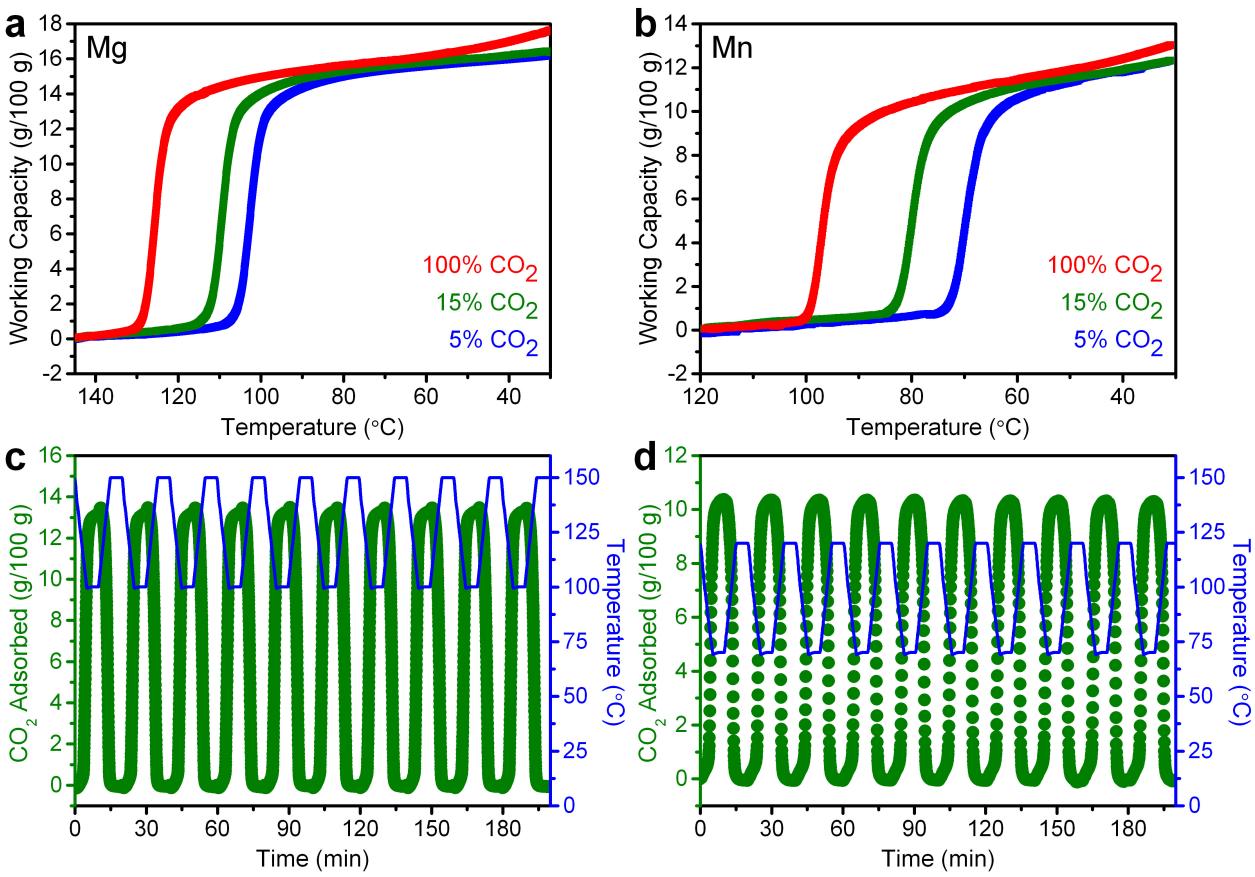


**Figure 6 | Isobaric $CO_2$ adsorption and regeneration energy comparisons. a-b**, Variable-temperature adsorption isobars of 100%, 15%, and 5% $CO_2$ (in $N_2$) for mmen-$Mg_2$(dobpdc) (**a**) and mmen-$Mn_2$(dobpdc) (**b**) demonstrate that under dynamic conditions the sharp transition region allows phase-change adsorbents to achieve very large working capacities under a wide range of adsorption conditions. For each material, the phase-transition temperature is dependent on the pressure of $CO_2$ in the gas mixture, with higher phase-transition temperatures observed at higher $CO_2$ partial pressures. (**c**) Cycling data for a pure temperature swing process involving adsorption from a simulated coal flue gas (15% $CO_2$ in $N_2$) at 100 °C in mmen-$Mg_2$(dobpdc) (**c**) and 70 °C in mmen-$Mn_2$(dobpdc) (**d**), followed by desorption at 150 and 120 °C, respectively, utilizing a flow of 100% $CO_2$. Respective working capacities of 13% and 10% are attained, with no loss in capacity over the course of ten cycles.

1. International Energy Agency, *$CO_2$ Emissions from Fuel Combustion: Highlights* (IEA, 2013; http://www.iea.org/publications/freepublications/publication/CO2EmissionsFromFuelCombustionHighlights2013.pdf).
2. IPCC, 2013: Summary for Policymakers, in: *Climate Change 2013: The Physical Science Basis. Contribution of Working Group I to the Fifth Assessment Report of the Intergovernmental Panel on Climate Change*, T. F. Stocker, *et al.* Eds. (Cambridge Univ. Press, New York, 2013).
3. Orr, J. C. *et al.* Anthropogenic ocean acidification over the twenty-first century and its impact on calcifying organisms. *Nature* **437**, 681 (2005).
4. Haszeldine, R. S. Carbon capture and storage: how green can black be? *Science* **325**, 1647 (2009).
5. Boot-Handford, M. E. *et al*. Carbon capture and storage update. *Energy Environ. Sci.* **7**, 130 (2014).
6. Choi, S.; Drese, J. H. & Jones, C. W. Adsorbent materials for carbon dioxide capture from large anthropogenic point sources. *Chem. Sus. Chem.* **2**, 796 (2009).
7. Lin, L. C. *et al*. In silico screening of carbon-capture materials. *Nat. Mater.* **11**, 633 (2012).
8. Sumida, K *et al*. Carbon dioxide capture in metal-organic frameworks. *Chem. Rev.* **112**, 724 (2012).
9. Zhou, H.C.; Long, J. R. & Yaghi, O. M. Introduction to metal-organic frameworks. *Chem. Rev.* **112**, 673 (2012).
10. Furukawa, H.; Cordova, K. E.; O'Keeffe, M. & Yaghi, O. M. The chemistry and applications of metal-organic frameworks. *Science* **341**, 123 (2013).
11. Demessence, A.; D'Alessandro, D. M.; Foo, M. L. & Long, J. R. Strong $CO_2$ binding in a water stable triazolate-bridged metal-organic framework functionalized with ethylenediamine. *J. Am. Chem. Soc.* **131**, 8784 (2009).
12. McDonald, T. M.; D'Alessandro, D. M.; Krishna, R. & Long, J. R. Enhanced carbon dioxide capture upon incorporation of *N*,*N*′-dimethylethylenediamine in the metal-organic framework CuBTTri. *Chem. Sci.* **2,** 2022 (2011).
13. McDonald, T. M. *et al*. Capture of carbon dioxide from air and flue gas in the alkylamine-appended metal-organic framework mmen-$Mg_2$(dobpdc). *J. Am. Chem. Soc.* **134**, 7056 (2012).
14. Hong, C. S. *et al*. Diamine-functionalized metal-organic framework: Exceptionally high $CO_2$ capacities from ambient air and flue gas, ultrafast $CO_2$ uptake rate, and adsorption mechanism. *Energy Environ. Sci.* **7**, 744 (2014).
15. Rosi, N. L. *et al.* Rod packings and metal-organic frameworks constructed from rod-shaped secondary building units. *J. Am. Chem. Soc.*, **127**, 1504 (2005).
16. Dietzel, P. D. C.; Panella, B.; Hirscher, M.; Blom, R. & Fjellvåg, H. Hydrogen adsorption in a nickel based coordination polymer with open metal sites in the cylindrical cavities of the desolvated framework. *Chem. Commun.* 969 (2006).
17. Caskey, S. R.; Wong-Foy, A. G. & Matzger, A. J. Dramatic tuning of carbon dioxide uptake via metal substitution in a coordination polymer with cylindrical pores. *J. Am. Chem. Soc.* **130**, 10870 (2008).
18. Mason, J. A. *et al*. Evaluating metal-organic frameworks for post-combustion carbon dioxide capture via temperature swing adsorption. *Energy Environ. Sci*. **4**, 3030 (2011).
19. Coelho, A. A. Whole-profile structure solution from powder diffraction powder using simulated annealing. *J. Appl. Crystallogr.* **33**, 899 (2000).
20. Planas, N. *et al.* The mechanism of carbon dioxide adsorption in an alkylamine-functionalized metal-organic framework. *J. Am. Chem. Soc.* **135**, 7402 (2013).

21. Tiritiris, I & Kantlehner, W. Orthoamide und Iminiumsalze, LXX [1]. Zur Fixierung von Kohlendioxid mit organischen Basen (Teil 1) – Reaktionen von Diaminen mit Kohlendioxid. *Z. Naturforsch.* **66b**, 164 (2011).
22. Drisdell, W.S. *et a*l. Probing adsorption interactions in metal-organic frameworks using X-ray spectroscopy. *J. Am. Chem. Soc.* **135**, 18183-18190 (2013).
23. Weiss, J. N. The Hill equation revisited: uses and misuses. *FASEB J.* **11**, 835 (1997).
24. Irving, H. & Williams, R. J. P. The stability of transition-metal complexes. *J. Chem. Soc.* **637**, 3192 (1953).
25. Perdew, J. P.; Burke, K. & Ernzerhof, M. Generalized gradient approximation made simple. *Phys. Rev. Lett.* **77**, 3865-3868 (1996).
26. Walton, K. S. *et al.* Understanding inflections and steps in carbon dioxide adsorption isotherms in metal-organic frameworks. *J. Am. Chem. Soc.* **130**, 406 (2008).
27. Horike, S.; Shimomura, S. & Kitagawa, S. Soft porous crystals. *Nat. Chem.* **1**, 695 (2009).
28. Serre, C. *et al.* Very large breathing effect in the first nanoporous chromium(III)-based solids: MIL-53 or $Cr^{III}(OH)\cdot\{O_2C–C_6H_4–CO_2\}\cdot\{HO_2C–C_6H_4–CO_2H\}_x\cdot\{H_2O\}_y$. *J. Am. Chem. Soc.* **124**, 13519 (2002).
29. Henke, S. *et al.* Multipe phase-transitions upon selective $CO_2$ adsorption in an alkyl ether functionalized metal-organic framework – an *in situ* X-ray diffraction study. *CrystEngComm*, **13**, 6399-6404 (2011).
30. Seo, J.; Matsuda, R.; Sakamoto, H.; Bonneau, C. & Kitagawa, S. A pillared-layer coordination polymer with a rotable pillar acting as a molecular gate for guest molecules. *J. Am. Chem. Soc.* **131**, 12792-12800 (2009).
31. Thomy, A. & Duval, X. Stepwise isotherms and phase transitions in physisorbed films. *Surf. Sci.* **299–300**, 415 (1994).
32. Jessop, P. G.; Mercer, S. M. & Heldebrant, D. J. $CO_2$-triggered switchable solvents, surfactants, and other materials. *Energy Environ. Sci.* **5**, 7240 (2012).
33. Liebenthal, U. *et al*. Overall process analysis and optimisation for $CO_2$ capture from coal fired power plants based on phase change solvents forming two liquid phases. *Energy Procedia* **37**, 1844 (2013).
34. Ma'mun, S. & Kim, I. Selection and characterization of phase-change solvent for carbon dioxide capture: precipitating system. *Energy Procedia* **37,** 331 (2013).
35. Choi, S.; Watanabe, T. Bae, T.-H.; Sholl, D. S. & Jones, C. W. Modification of the Mg/DOBDC MOF with amines to enhance $CO_2$ adsorption from ultradilute gases. *J. Phys. Chem. Lett.* **3**, 1136-1141 (2012).
36. Rochelle, G. *et al*. Aqueous piperazine as the new standard for $CO_2$ capture technology. *Chem. Eng. J.* **171**, 725 (2011).
37. Sayari, A. & Blemabkhout, Y. Stabilization of amine-containing $CO_2$ adsorbents: dramatic effect of water vapor. *J. Am. Chem. Soc.* **132**, 6312 (2010).
38. Nugent, P. *et al*. Porous materials with optimal adsorption thermodynamics and kinetics for $CO_2$ separation. *Nature* **495**, 80-84.
39. van Lare, C. E. J. Thesis, Technische Universiteit Eindhoven (1991).
40. Lorimer, G. The carboxylation and oxygenation of ribulose 1,5–bisphosphate: the primary events in photosynthesis and photorespiration. *Annu. Rev. Plant Physiol.* **32**, 349 (1981).
41. Taylor, T. C. & Andersson, I. Structural transitions during activation and ligand binding in hexadecameric Rubisco inferred from the crystal structure of activated unliganded spinach enzyme. *Nat. Struct. Biol.* **3**, 95 (1996).
42. Assche, F. & Clijsters, H. Effects of metals on enzyme activity in plants. *Plant Cell Environ.* **13**, 195 (1990).

**Supplementary Information** is available in the online version of the paper.

**Acknowledgements** The work presented here pertaining to the synthesis and gas adsorption properties of metal-organic frameworks was funded by the Advanced Research Projects Agency-Energy (ARPA-E), U.S. Department of Energy, under Award Numbers DE-AR0000103 and DE-AR0000402. Funding pertaining to the characterization of materials by spectroscopic, x-ray diffraction, and computational methods was provided by the Center for Gas Separations Relevant to Clean Energy Technologies, an Energy Frontier Research Center funded by the U.S. Department of Energy, Office of Science, Office of Basic Energy Sciences under award DE-SC0001015. Experiments performed in Turin were additionally supported by grant MIUR-PRIN 2010-2011. We thank Prof. Kenneth Suslick for valuable discussions and Dr. Lynn Ribaud and the 11-BM staff at the Advanced Photon Source at Argonne National Laboratory for assisting with powder x-ray diffraction experiments. Use of the Advanced Photon Source at Argonne National Laboratory was supported by the U. S. Department of Energy, Office of Science, Office of Basic Energy Sciences, under Contract No. DE-AC02-06CH11357. We further thank the National Science Foundation for fellowship support of J.A.M., and Gerald K. Branch and Arkema for fellowship support of E.D.B.

**Author Contributions** T.M.M. and J.R.L. formulated the project. T.M.M., E.D.B. and D.G. synthesized the compounds. T.M.M. collected and analysed the gas adsorption data. J.A.M. collected and analysed the x-ray diffraction data. X.K. collected the NMR data. X.K. and J.A.R. analysed the NMR data. T.M.M., V.C., F.G. and S.B. collected and analysed the IR data. W.D. and J.B.K. collected and analysed the XAS data. S.O., B.V., A.L.D., R.P., S.K.S., N.P., L.K. and T.P. performed the computations and analysed the results. D.P., J.B.N., B.S. and L.G. helped with the computational analyses. T.M.M., J.A.M. and J.R.L. wrote the paper, and all authors contributed to revising the paper.

**Author Information** Reprints and permissions information is available at www.nature.com/reprints. The authors and the University of California have filled for a patent on some of the results contained herein. Readers are welcome to comment on the online version of the paper. Correspondence and requests for materials should be addressed to J.R.L (jrlong@berkeley.edu).